Influences of solid and lubricant thermal conductivity on traction in an EHL circular contact

H.C. Liu, B.B. Zhang, N. Bader, G. Poll, C.H. Venner

PII: S0301-679X(19)30574-2

DOI: https://doi.org/10.1016/j.triboint.2019.106059

Reference: JTRI 106059

To appear in: *Tribology International*

Received Date: 11 September 2019

Revised Date: 29 October 2019

Accepted Date: 1 November 2019

Please cite this article as: Liu HC, Zhang BB, Bader N, Poll G, Venner CH, Influences of solid and lubricant thermal conductivity on traction in an EHL circular contact, *Tribology International* (2019), doi: https://doi.org/10.1016/j.triboint.2019.106059.

Manuscript submitted to *Tribology International*

Title:

Influences of solid and lubricant thermal conductivity on traction in an EHL circular contact

Authors:

H.C. Liu[1*], B.B. Zhang[2], N. Bader[1], G. Poll[1], C.H. Venner[2]

[1] Institute of Machine Design and Tribology, University of Hannover, 30167 Hannover, Germany

[2] Faculty of Engineering Technology, University of Twente, 7500AE Enschede, the Netherlands

*Correspondence author:

HaiChao Liu

E-mail: liu@imkt.uni-hannover.de

Address: IMKT, University of Hannover, 30167 Hannover, Germany

Abstract

The influences of thermal conductivity of both the contacting solids and the lubricant on the traction in a rolling/sliding EHL contact have been studied numerically. For through-hardened AISI 52100 bearing steel (k was measured as $21\ \mathrm{W/mK}$ by Reddyhoff et al., see Tribol Lett $67(1): 22, 2019$), with the improper but widely used thermal conductivity of $46\ \mathrm{W/mK}$ in literature, the friction coefficient can be overestimated and the maximum temperature in the lubricating film would be underestimated. The effect of solid thermal conductivity on traction depends on the entrainment speed and the resulting film thickness. For the thermal conductivity of the lubricant, its pressure dependence affects the traction mainly at high speeds and/or at high sliding-to-rolling ratio (SRR) conditions.

Keywords

Thermal conductivity; Thermal EHL; Traction; Bearing steel

1 Introduction

Film thickness and traction are two important factors concerning elastohydrodynamic lubrication (EHL). EHL film thickness can be predicted fairly well with numerical solutions [1] or analytical formulae fit to numerical solutions [2, 3], while for EHL traction, there are considerable discrepancies between measurements and the results of full numerical simulation [4]. EHL film thickness is determined by the amount of oil that is entrained into the contact zone in the inlet region, where pressure and shear stress are relatively low. The isothermal assumption mostly holds for the film thickness prediction. Only under severe operating conditions, *e.g.* high speeds or high loads, inlet shear heating can reduce the inlet oil viscosity with a consequent reduction in film thickness [5]. In contrast, EHL traction is determined by the shear properties of the lubricant in the high pressurized contact zone, where the viscosity and thus the stress needed to shear the fluid would be high. Under such a high shear stress, the lubricant seldom behaves Newtonian, and shear thinning, limiting shear stress and shear heating may occur [6]. As a result, thermal and non-Newtonian effects cannot be ignored for traction prediction.

Many fluid models have been proposed for the purpose of EHL traction prediction, see references [6-8] as examples. However, it should be noted that which fluid model can best describe the EHL film behavior under high pressure and high shear stress is still an open question. For the validation of the models, traction machines, either twin-disc machines or ball-on-disc test rigs, are widely employed to measure the EHL traction. Even with a well characterized lubricant, the deviation of traction curves between simulation and experiments is still obvious [4]. There are many possible reasons for this, *e.g.* the necessity of accurate estimation of the limiting shear stress [9], the solid body temperature effect pointed out by Björling et al. [4] and analyzed recently by the current authors [10]. Besides these, one underlying reason can be the improper thermal conductivity values adopted for both the contacting solids and the lubricant in the thermal EHL (TEHL) simulation. The specimens of the traction machine are typically made of AISI 52100 bearing steel. Recently, Reddyhoff et al. [11] measured the thermal conductivity of through-hardened AISI 52100 steel specimens employed in a traction machine with a frequency domain thermoreflectance (FDTR) method. For both the ball and the disc, the thermal conductivity value is $21\ \mathrm{W/mK}$, which is less than half of the value (about $46\ \mathrm{W/mK}$) commonly used in the TEHL simulations for the traction of an AISI 52100 steel contact, see Refs. [4,10,12,13]. Reddyhoff et al. show that the discrepancy may result from through-hardening of the steel, which leads to thermal conductivity

reduction. It is important and interesting to understand the influences of steel thermal conductivity on EHL traction and temperature rise.

Apart from the solid thermal conductivity, the thermal conductivity of the lubricant may play an important role on EHL traction and film temperature distribution as well. Larsson and Andersson [14] measured the thermal conductivity for various oils under elevated pressures using the transient hot-wire method. Their results showed that for all measured lubricants the thermal conductivity at 1 GPa is at least two times larger than the value at atmospheric pressure. Larsson and Andersson [14] gave an empirical equation to describe the pressure dependence of the oil thermal conductivity. Similar phenomenon has also been reported by Bair and Andersson et al. [15] for a reference liquid, squalane. However, in classical TEHL simulations, the oil thermal conductivity is assumed to be independent of pressure, and the value at atmospheric pressure is employed (about $0.14\ \mathrm{W/mK}$). This means a smaller thermal conductivity is employed in the simulations than it should be. Consequently, less heat can be conducted to the surfaces and hence the temperature rise in the film is higher, which leads to underestimation of the predicted friction coefficient. This kind of influence has been shown by Habchi et al. in a quantitative TEHL simulation with Shell T9 mineral oil by considering the real thermal conductivity behavior of the oil [12]. Their traction simulation results agreed with the measurements on a ball-on-disc traction machine. However, in the TEHL simulation, the thermal conductivity of the bearing steel was used as $50\ \mathrm{W/mK}$ (Table 1 in [12]), which is over two times larger than the new measured value of $21\ \mathrm{W/mK}$.

In this study, the influences of solid and lubricant thermal conductivity on EHL traction and temperature rises are investigated numerically for a steel-steel point contact problem. Squalane, which may be the best characterized reference fluid for EHL study, is employed for the analysis. The role of steel thermal conductivity on traction is shown in Sec.4.1. Sec.4.2 studies the influences of oil thermal conductivity on EHL traction. The simulated traction results are compared with the measurements from a traction machine and the measurements by Björling et al. with the same liquid [16]. Finally, the effect of thermal conductivity on EHL film thickness and the reliability of the thermal reduction factor [17] will be briefly discussed.

2 Theoretical models

Numerical simulation of the traction in a rolling/sliding thermal EHL contact requires the modelling of several phenomena simultaneously: thin film flow (*e.g.* Reynolds equation), deformation of the surfaces (*e.g.* elastic half space model), fluid models (*e.g.* viscosity-pressure-temperature relation, shear thinning and limiting shear model), and thermal parts (*e.g.* oil-solid energy equations). The EHL governing equations and the energy equations can be found in Appendix 1 or elsewhere. The rheological model and fluid properties used in the current study will be recalled in this section.

As is suggested by Bair et al. [18], preliminary measurements of the thermal-physical properties of the lubricants are essential for the quantitative simulation of EHL behavior. Squalane, whose properties (viscosity, thermal conductivity and heat capacity) have been thoroughly measured by Bair and co-workers [4,15,19,22] and thereafter fitted to physical models, is chosen. The viscosity was measured up to 1.5 GPa at a wide temperature range and the data was fitted to free-volume based models, in which the fast-than-exponential behavior can be seen [15]. In Ref.[15], there are several free volume models available to describe the low shear viscosity of squlane, which basically yield the same viscosity results

until a pressure of 1.25 GPa. The Murnaghan equation of state [23] for density and the improved Yasutomi correlation [24] for viscosity are adopted in this work (see Table 1). The measured shear dependence of viscosity agrees with molecular dynamic simulation results, and the behavior is described by a *t-T-p* shifted Carreau-type shear thinning model [19]. The pressure dependence of the thermal conductivity of squalane was also reported in Ref.[15] and its effect on EHL traction will be studied. The used fluid models and parameters for squalane are summarized in Table 1.

Table 1 Fluid models and parameters of squalane oil (all the parameters came from Ref. [4,15,19,22]. Subscripts R indicates a reference state, i.e. $p_{\mathrm{R}} = 0$ and $T_{\mathrm{R}} = 40$ °C)

Fluid models	Parameters
1. Shear thinning: Carreau equation [19] $\eta^*(\dot{\gamma}, p) = \mu\left[1 + \left(\dot{\gamma}_{\mathrm{e}}\lambda_{\mathrm{R}}\frac{\mu}{\mu_{\mathrm{R}}}\frac{T_{\mathrm{R}}}{T}\frac{V}{V_{\mathrm{R}}}\right)^2\right]^{(n-1)/2}$	$\mu_{\mathrm{R}} = 15.6$ mPas, $\lambda_{\mathrm{R}} = 2.26 \times 10^{-9}$ s, and $n = 0.463$
2. Density: Murnaghan equation of state [23] $\rho = \frac{\rho_{\mathrm{R}}}{1+\alpha_{\mathrm{V}}(T-T_{\mathrm{R}})} \times \left(1 + \frac{K_0'}{K_0}p\right)^{\frac{1}{K_0'}}$, with $K_0 = K_{00}\exp(-\beta_{\mathrm{K}}T)$	$K_0' = 10.85$, $\alpha_{\mathrm{V}} = 8.35 \times 10^{-4}$ K^{-1}, $K_{00} = 8.824$ GPa, $\rho_{\mathrm{R}} = 795.8$ kg/m^3, $\beta_{\mathrm{K}} = 6.321 \times 10^{-3}$ K^{-1}
3. Low shear viscosity: Yasutomi equation [24] $\mu = \mu_{\mathrm{g}}\exp\left[\frac{-2.303C_1(T-T_{\mathrm{g}})F}{C_2+(T-T_{\mathrm{g}})F}\right]$ with $T_{\mathrm{g}} = T_{\mathrm{g0}} + A_1\ln(1 + A_2p)$ and $F = (1 + B_1p)^{B_2}$	$A_1 = 263.8$ °C, $A_2 = 0.3527$ GPa^{-1}, $B_1 = 13.73$ GPa^{-1}, $B_2 = -0.3426$, $C_1 = 11.66$, $C_2 = 39.17$ °C, $T_{\mathrm{g0}} = -88.69$ °C, $\mu_{\mathrm{g}} = 1.23 \times 10^7$ Pas
4. Thermal conductivity: empirical equation [4] $k_{\mathrm{oil}} = C_{\mathrm{k}}\kappa^{-s}$, with a scaling parameter $\kappa = \left(\frac{V}{V_{\mathrm{R}}}\right)\left[1 + A\left(\frac{T}{T_{\mathrm{R}}}\right)\left(\frac{V}{V_{\mathrm{R}}}\right)^q\right]$	$A = -0.115$, $C_{\mathrm{k}} = 0.074$ W/mK, $s = 4.5$, $q = 2$
5. Thermal capacity: empirical equation [4] $C = C' + m\chi$, with $\chi = \left(\frac{T}{T_{\mathrm{R}}}\right)\left(\frac{V}{V_{\mathrm{R}}}\right)^{-3}$	$C' = 0.94 \times 10^6$ J/ m^{3}K, $m = 0.62 \times 10^6$ J/ m^{3}K
6. Limiting shear stress [19]: assumed relation $\tau_{\mathrm{L}} = \Lambda p$	$\Lambda = 0.075$

3 Numerical solutions

3.1 Numerical methods

The above equations were rewritten in dimensionless forms, and subsequently, they were discretized with finite difference method. See nomenclature for the non-dimension parameters.

The computation is achieved iteratively between pressure-film fields (PH cycles) and temperature-shear rate fields ($\bar{T}\dot{\Gamma}$ cycles). The Reynolds equation for pressure distribution and the double integral for surface deformation are solved efficiently by the multigrid method and the multilevel multi-integration method [1], respectively. The temperatures are solved with a column-by-column relaxation scheme introduced by Yang [25]. The TEHL simulation program used in this study was originally written by Guo and Yang [26] at Qindao University of Technology and it was updated by Liu and Zhang et al. [10] through implementations of various fluid models for the purpose of traction prediction and fluid model validation with reference fluids (*e.g.* Shell T9, squalane, DEHS). Limiting shear stress was also implemented using the same method as Habchi [12,16], that is, during the iterative computation process, the local shear stress $\tau(x,y,z)$ was continuously checked to meet $\tau(x,y,z) \le \tau_L$; and if $\tau(x,y,z) > \tau_L$, then let $\tau(x,y,z) = \tau_L$.

The calculation domain was $-9.0 \le X \le 1.6$, and $-3.4 \le Y \le 3.4$, where 513 nodes distributed equally on the finest level of grid (level 5) in both the *X*- and *Y*- directions. The number of nodes used for solving the 3D energy equations was 10 with equal distances across the film, and 8 with non-equal distances in each solid. The heat penetration depth or the computation boundary $D = d/a = 6.3$ was checked as sufficiently far from the solid-oil interface. The *D* value here is two times larger than that used by Yang [25,26] and Habchi [27]. Further expanding the *D* value of heat penetration or refining the mesh density has negligible effect on the accuracy of the calculated temperature and friction coefficient for the operating conditions in this study. The convergence criterions are:

$$\begin{cases} \sum \left| P_{i,j}^{(new)} - P_{i,j}^{(old)} \right| / \sum P_{i,j}^{(new)} < 0.001 \\ \sum \left| \bar{T}_{i,j,k}^{(new)} - \bar{T}_{i,j,k}^{(old)} \right| / \sum \bar{T}_{i,j,k}^{(new)} < 0.0001 \\ \sum \left| \dot{\Gamma}_{i,j,k}^{(new)} - \dot{\Gamma}_{i,j,k}^{(old)} \right| / \sum \dot{\Gamma}_{i,j,k}^{(new)} < 0.001 \\ \left| \sum P_{i,j}^{(new)} \mathrm{d}X\mathrm{d}Y - \frac{2\pi}{3} \right| / \left(\frac{2\pi}{3} \right) < 0.001 \end{cases}$$

3.2 Model Validation

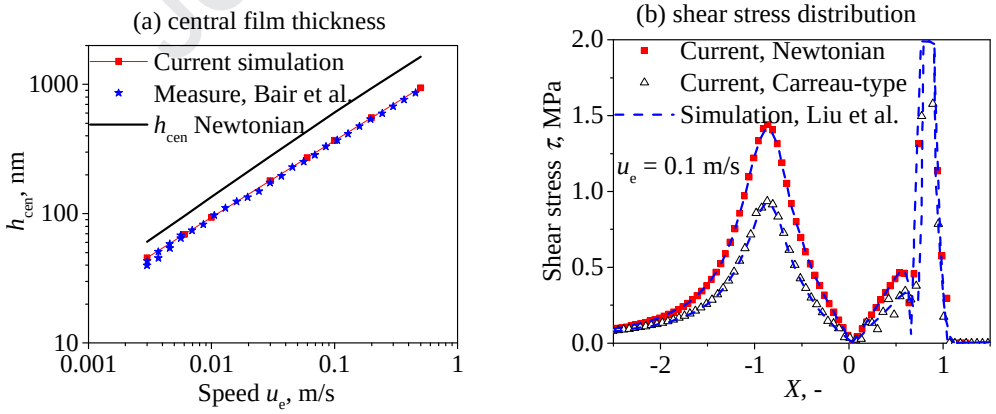

Fig.1 Comparison between current simulation and results in literature [21,28] (PAO650, $T_0 = 75$ °C, $p_H = 0.528$ GPa, pure rolling)

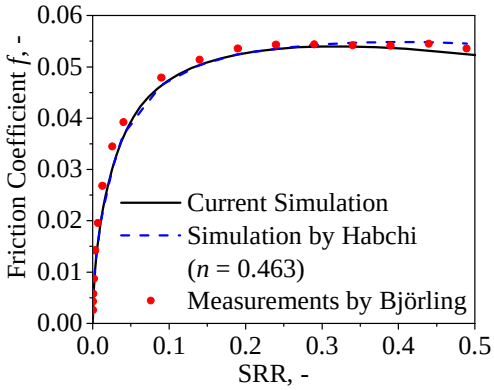

Fig.2 Traction curve comparison between current simulation and results in literature [29] (squalane, $T_0 = 40$ °C, $p_{\mathrm{H}} = 1.07$ GPa, $k_{\mathrm{s}} = 46$ W/mK, $k_{\mathrm{oil}}(p,T)$)

Figure 1 compares the film thickness and shear stress distribution from the current thermal EHL model with the results from Refs. [21,28] with PAO650. The calculated central film thicknesses in Fig.1(a) agree with the measured values in Ref. [28]. They are smaller than the results with Newtonian fluid model. Fig.1(b) shows that the calculated shear stress distributions agree with the simulation by Liu et al. [21]. In the inlet region, the calculated shear stress with Carreau shear thinning is smaller than that with Newtonian fluid model. Inlet shear thinning does occur for PAO650 under pure rolling conditions. Figure 2 shows the comparison of traction curves for squalane. Generally, the current result agrees with the finite element simulation done by Habchi and the measurements done by Björling et al. in Ref. [29].

4 Results and discussion

Rolling/sliding circular contacts of a ball-on-disc traction rig lubricated with squalane are modeled. Both the ball and the disc are made of bearing steel. The supplied oil temperature is 40 °C and the Hertzian contact pressure is 1.25 GPa. The input parameters for the simulation are given in Table 2.

Table 2 Material thermal-physical properties and operating conditions

Item/Property	Value
Bearing Steel	
Young's modulus E	210 GPa
Poisson ratio	0.3 (-)
Heat capacity $c_{1,2}$	470 J/(kgK)
Thermal conductivity, k_{s}	21 and 46 W/(mK)
Density ρ	7850 kg/m^3
Squalane	
Viscosity η at 40°C, $p = 0$	0.015 Pas
Densityρ at 40°C, $p = 0$	795.8 kg/m^3
Viscosity-pressure coefficient α at 40°C	18 GPa^{-1}
Thermal conductivity k_{oil} at 40°C, $p = 0$	0.1282 W/(mK)
Heat capacity c at 40°C, $p = 0$	1960.3 J/(kgK)
Operating conditions	
Effective radius $R = R_{\mathrm{x}} = R_{\mathrm{y}}$	10.314 mm
Supplied oil and solid body temperature T_0	313 K(40 °C)
Load w	80 N

Hertz contact pressure p_{H}	1.25 GPa
Entrainment speed u_{e}	0.1-10 m/s
Slide-to-roll ratio (SRR), ξ	0-100%

4.1 Effect of solid thermal conductivity

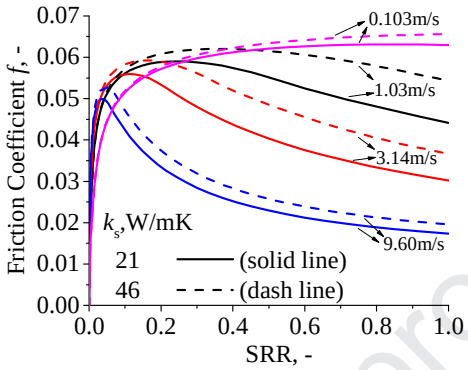

Fig.3 Traction curves with two solid thermal conductivities of $k_s = 21$ W/mK (solid lines) and 46 W/mK (dash lines), respectively, at four entrainment speeds in a circular EHL contact. (squalane, $T_0 = 40$ °C, $p_{\mathrm{H}} = 1.25$ GPa; 21 W/mK was measured by Reddyhoff et al. [11] for hardened AISI 52100 steel, while 46 W/mK is the common cited but improper value in thermal EHL literature.)

Two thermal conductivities, k_s, of the AISI 52100 bearing steel are employed. 21 W/mK is the thermal conductivity of hardened AISI 52100 bearing steel measured by Reddyhoff et al., and 46 W/mK represents the thermal conductivity that was usually adopted in the TEHL simulations for traction tests. Figure 3 compares the calculated traction curves for the two solid thermal conductivities over a wide SRR range at four velocities. For each group of traction curves of the same thermal conductivity, the friction coefficient decreases at moderate and large SRRs with the increasing speed. This is simply due to enhanced heat generation at a higher entrainment speed. For the same speed, the traction curve can be highly influenced by the solid thermal conductivity. With the smaller thermal conductivity of 21 W/mK, less heat could be conducted out the film, which leads to higher film temperature rise and thus lower viscosity and smaller friction coefficient. The maximum oil temperature rises for the two thermal conductivities with the variation of SRR are shown in Fig.4. The smaller solid thermal conductivity gives the larger temperature rise within the EHL film and then the friction reduction behavior in Fig.3. This friction reduction phenomenon using two solid thermal conductivities looks similar to the work done by Björling et al. by coating the steel surface with a low thermal conductivity material, *e.g.* an insulating DLC coating [16].

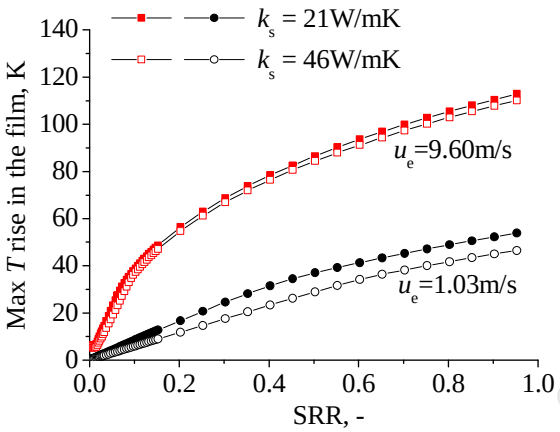

Fig.4 Maximum oil temperature rise for two thermal conductivities at a low entrainment speed of 1.03 m/s and a high speed of 9.60 m/s. The running conditions are the same as that in Fig.3. (squalane, $T_0 = 40$ °C, $p_H = 1.25$ GPa)

An unexpected phenomenon is that the solid thermal conductivity influences both the traction (Fig.3) and the temperature rise (Fig.4) more obviously at a relatively low entrainment speed of 1.03 m/s, but not at a high speed of 9.60 m/s where more heat is generated. This is especially the case for the traction at high SRRs. The distributions of the mid-film and the two surface temperatures along the central line of the contact (plane $Y = 0$) are depicted in Fig.5 for cases of 1.03 m/s and 9.60 m/s corresponding to Fig.3 at SRR = 50%. It shows the same trend, that is, at the low speed of 1.03 m/s the temperature difference of mid-film temperature at two thermal conductivities is larger than that at 9.60 m/s. This may be explained by the differences in film thickness. As is known, EHL film is sensitive to entrainment speed ($h_{cen} \propto U_e^{0.67}$), and the thermal conductivity of oil is quite low (*e.g.* 0.13 W/mK at ambient pressure), which is around hundred times smaller than that of the bearing steel. This means that for the generated heat near the center plane of the film it is hard to reach the solid surface and then conduct out from the rather thick film caused by a high speed. The calculated central film thicknesses are 124.3 nm and 505.1 nm for the two speeds, respectively. It can be seen from Fig.5 that with the same k_s value of 21 W/mK, the difference between mid-film temperature and any of the two surface temperatures is smaller for the low film thickness case (low speed case, Fig.5a) than that for the thick film thickness case (high speed case, Fig.5b). As can be imagined, if the film thickness is thick enough or the speed is high enough, the heat is mainly kept in the EHL film (thermal and shear localization in the mid-film) and the solid thermal conductivity has almost no influence on traction and maximum temperature rise. From Fig.3 and the above analysis, it can be know that the effect of the solid body temperature on traction is of speed or film thickness dependence.

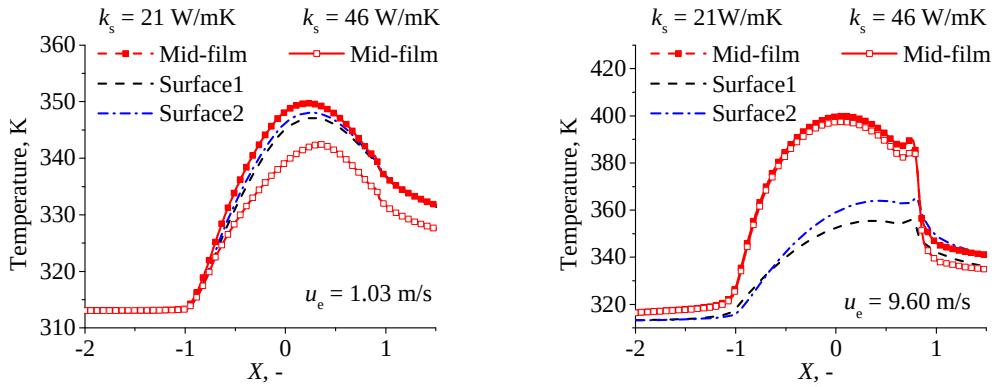

(a) low speed case of 1.03 m/s (b) high speed case of 9.60 m/s

Fig.5 Temperature distribution for two thermal conductivities at a low entrainment speed and a high speed. The running conditions are the same as that in Fig.3 with SRR = 50%. Plane $Y = 0$. (squalane, $T_0 = 40$ °C, $p_H = 1.25$ GPa)

4.2 Effect of lubricant thermal conductivity

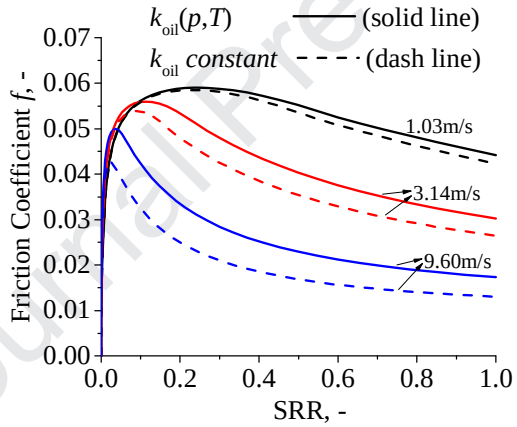

Fig.6 Influences of pressure dependence of lubricant thermal conductivity on traction at three entrainment speeds in a circular EHL contact. (squalane, $T_0 = 40$ °C, $p_H = 1.25$ GPa, $k_s = 21$ W/mK)

To evaluate the effect of pressure dependence of thermal conductivity, traction curve calculations are carried out by setting the liquid thermal conductivity to a constant value of 0.1282 W/mK ($p = 0$, 40 °C) or by using the equation in Table 1 to consider its pressure dependence. The two cases are labeled as $k_{oil}(p,T)$ and $k_{oil}\ constant$, respectively. The calculated traction curves for those two cases are compared in Fig.6. After considering the $k_{oil}(p,T)$ relation, the friction coefficient becomes larger than that of $k_{oil}\ constant$, because more heat can conduct through the film to the solids. In other words, the EHL traction can be underestimated by simply ignoring the pressure and oil thermal conductivity relation, especially at high SRRs and/or at high speed running conditions. Similar phenomenon has been reported by Habchi et al. [12] with TEHL simulation using Shell T9 mineral oil. It should be mentioned that the thermal conductivity of squalane increases dramatically with increasing pressure, whereas there is only slight change in terms of temperature [15]. Hence, the thermal conductivity may be regarded as pressure dependent only.

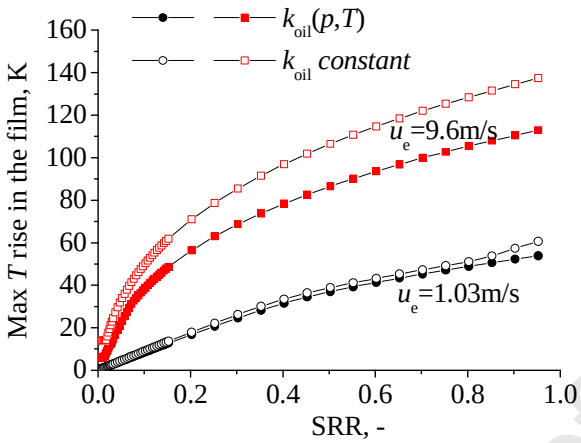

Fig.7 Influences of pressure dependence of lubricant thermal conductivity on maximum oil temperature rise at a low entrainment speed and a high speed. The running conditions are the same as that in Fig.6. (squalane, $T_0 = 40$ °C, $p_H = 1.25$ GPa, $k_s = 21$ W/mK)

As can be seen in Fig.6, this kind of pressure-enhanced liquid thermal conductivity effect on traction is obvious for the high entrainment speed condition rather than for the low speed condition, which is different from the influence of solid thermal conductivity in Fig.3 of Sec.4.1. All heat is originally generated in the film, *e.g.* mainly by shear heating. With a low speed, the amount of generated heat is small and its distribution across the resulting thin film is almost regardless of the changes in lubricant thermal conductivity. This can be seen in Fig.7 that there is almost no temperature difference for the low speed case. Indeed, the temperature distribution is mainly controlled by the solid thermal conductivity for a thin film, as is shown in Fig.3 ($u_e = 1.03$ m/s). As a contrast, at a high entrainment speed and therefore a thick EHL film, the amount of heat generation is rather large. The increase in lubricant thermal conductivity would enhance the heat diffusion from the mid-plane of the film towards the solids through heat conduction. As a result, when the pressure and temperature dependence of thermal conductivity is considered for the high speed case, the maximum temperature rise near the mid-film should be lower (see Fig.7, the high speed case), while the temperature of the two solid surfaces should be higher than the results obtained with *k constant*, due to heat redistribution across the film (see Fig.8).

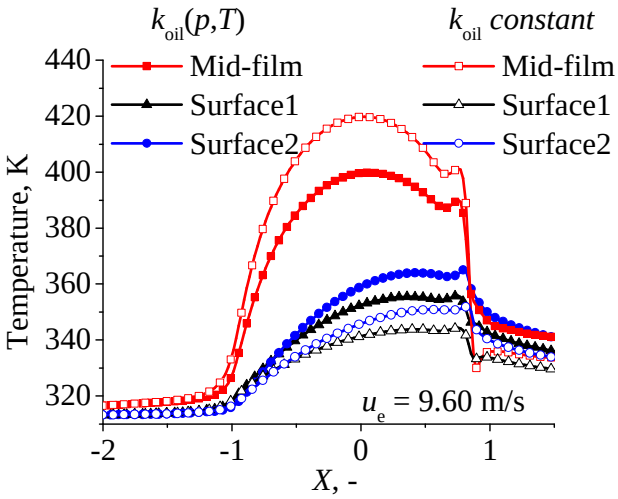

Fig.8 Temperature distributions of mid-film and two solid surfaces with the influences of lubricant thermal conductivity at a high speed. The running conditions are the same as that in Fig.6 with SRR = 50%. Plane $Y = 0$. (squalane, $T_0 = 40$ °C, $p_H = 1.25$ GPa, $k_s = 21$ W/mK, $u_e = 9.60$ m/s)

4.3 Traction comparison with experiments

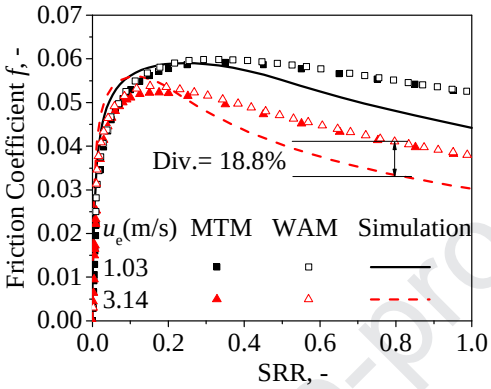

Fig.9 Quantitative traction curve comparison with squalane at two speeds. The traction curves were measured by two traction machines. ($T_0 = 40$ °C, $p_H = 1.25$ GPa, $k_s = 21$ W/mK, $k_{oil}(p,T)$)

Björling et al. [4,16] once measured the traction curves for squalane on a WAM ball-on-disc traction machine. The ball and disc are made of AISI 52100 steel, but there is no measurement of the thermal conductivity of these specimens. The samples measured by Reddyhoff et al. are specified for the MTM ball-on-disc traction machine. For this reason, traction measurements were also carried out with a MTM machine at VW Wolfsburg by the authors. The running conditions are the same as the conditions adopted in the simulation (Sec.4.1, Table 2).

Roller compliance can contribute to the SRR under high pressure [30,31]. The surface elastic slip of the ball and disc is corrected for the measured traction curves using the following equation suggested by Bair and Kotzalas [31] to give a pure fluid traction behavior.

$$\mathrm{SRR}_{\mathrm{fluid}} = \mathrm{SRR}_{\mathrm{total}} - f\frac{p_H}{G_s}$$

where f is the friction coefficient, G_s the shear modulus of steel (78 GPa used here). The corrected traction curves from the MTM and WAM traction rigs are compared with the simulation results in Fig.9. The traction measurement results from the two test rigs agree well for the operating conditions. The simulated traction curves capture all the features of the experimental curves. However, the largest deviation can be as high as 18.8% when they are compared quantitatively.

Surface roughness cannot be the main reason for the difference in Fig.9. The combined root mean square (RMS) roughness is about 14 nm for the MTM ball-on-disc contact. The minimum film thickness at the lower speed of 1.03 m/s is 69 nm, which is over three times larger than the combined roughness. Moreover, the amplitude of the roughness can be reduced due to EHL contact pressure. In such a full film condition, the effect of surface roughness on traction could be ignored. The reasons may lie in the accuracies of the fluid models, such as viscosity at high shear rate and high pressure and the pressure and

possible temperature dependence of limiting shear stress. The detailed analysis requires comparison over a wide speed and load operating conditions, which is out the range of this study.

4.4 Effect of thermal conductivity on film thickness- thermal reduction factor

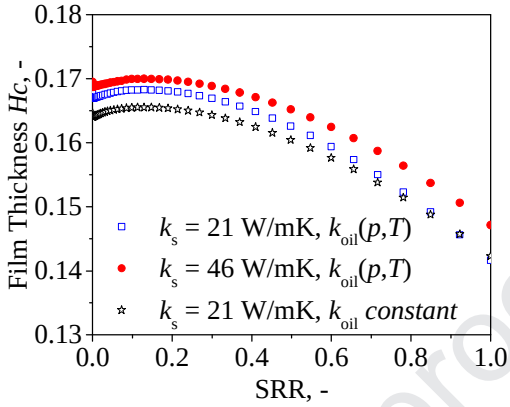

Fig.10 Non-dimensional central film thickness at different SRRs with different solid thermal conductivities and lubricant thermal conductivities. (squalane, $T_0 = 40\ ^\circ\mathrm{C}$, $p_\mathrm{H} = 1.25$ GPa, $u_\mathrm{e} = 9.60\ \mathrm{m/s}$)

As is known, inlet heating reduces the film thickness at a high speed even for pure rolling. This attributes to the shear heating effect caused by the reverse flow and heat convection effect in the inlet region. Both the solid and the lubricant thermal conductivities should affect the inlet temperature rise through inlet heat dissipation and then affect the inlet oil viscosity and EHL film thickness. There are several semi-empirical thermal reduction factors (TRF) available to account for the inlet thermal effect for line contacts [17]. The oil thermal conductivity has been embodied in the TRFs, while there is no variable related to the thermal conductivity of the contacting solids. Therefore, it is necessary to evaluate the influences of solid thermal conductivity on EHL film thickness.

For a circular steel-steel contact working at a high speed of $9.60\ \mathrm{m/s}$, the dimensionless central film thicknesses, $H_c = h_{cen}R_x/a^2$, are plotted in Fig.10 for three cases at different SRRs. In the first case, the solid thermal conductivity is $21\ \mathrm{W/mK}$ and the temperature and pressure dependence of lubricant thermal conductivity is also considered. The central film thickness calculated from the first case is regarded as the most accurate results and works as a reference for the other two cases. The other two cases are simulated either by changing the k_s to the value of $46\ \mathrm{W/mK}$ or by setting the k_oil as a constant. As can be seen in the figure, the case of $k_\mathrm{s} = 21\ \mathrm{W/mK}$ and k_oil *constant* gives the lowest film thickness, as both the solid and the liquid thermal conductivities contribute to increase the inlet film temperature. The largest deviation among different cases is less than 3% over all the calculation ranges. This may be neglected for engineering applications. Therefore, for steel-steel circular contacts, the solid thermal conductivity and the $k_\mathrm{oil}(p,T)$ relation are not important for the prediction of EHL film thickness concerning inlet shear heating.

The isothermal EHL central film thickness can be calculated simply by turning off the thermal calculation function in the program. For pure rolling $(\mathrm{SRR} = 0)$, it is 0.182 in dimensionless form. Accordingly, the result of thermal EHL simulation is 0.167, which is 8.24% smaller than the isothermal one. In Fig.10, the central film thickness firstly increases slightly to a maximum value and then decreases

with SRR. The increase of central film thickness at small and moderate SRRs may be attributed to the thermal expansion of the lubricant [32].

4.5 Outlook and Suggestions

On the thermal conductivity of AISI 52100 bearing steel, one can find different values in different literature and catalogs, usually ranging from 19 W/mK to 55 W/mK. The thermal conductivity is influenced by heat treatment and the phase composition of the steel [33]. There is usually retained austenite with controlled content in AISI 52100 bearing steel. The thermal conductivity of austenite phase is smaller than that of the martensite phase, and they are reported as 16.8 W/mK and 39.3 W/mK, respectively, in Ref.[34] at ambient conditions. Note that Habchi and Bair [35] provided a brief literature review on the thermal conductivity of steel, recently. Thermal conductivity depends on the hardness of the steel and it is around 21 W/mK for through-hardened AISI 52100 steel. Through thermal EHL simulation using Shell-T9 oil, they found that the friction coefficient is significantly overestimated in the thermo-viscous friction regime when the improper value of 46 W/mK is adopted. In this work, we did simulation over a wide range of speeds and found that the effect of solid thermal conductivity depends on the entrainment speed and the EHL film thickness. It is not obvious for either extra low speed or extra high speed conditions at high SRRs, whereas it is important for the traction at moderate entrainment speeds. At high speeds, the influence of solid thermal conductivity on traction is decreasing in the thermo-viscous regime, while its effect on the maximum friction coefficient is still noticeable for the traction curve (Fig.3).

During the service life of machine elements or even during manufacturing, there may be oxidization or tribo-layer formation on the surface or in a zone adjacent to the surface, the thermal property of which will differ from the bulk material. This would also influence the temperature rise in the film and also the traction behavior. The FDTR technique for measuring near-surface thermal conductivity introduced by Reddyhoff et al. [11] will be important and necessary for temperature and traction prediction. Before traction tests with a traction rig, the thermal conductivities of the ball and the disc are suggested to be measured.

In literature, Kaneta and Yang did TEHL analysis with different solid materials, mainly glass-to-steel of the optical EHL rig, to show the thermal wedge mechanism on dimple formation [36,37]. In this study, only a steel-steel contact was simulated, in which the influence of the solid thermal conductivity on the thermal correction factor and on the pure rolling film thickness seems to be not important. However, if the same conclusion can be drawn for the ceramic-steel contact in a high speed ceramic rolling bearing is still a question to be answered.

5 Conclusions

The influences of solid and lubricant thermal conductivities on EHL traction, temperature distribution and film thickness have been investigated with a non-Newtonian TEHL model for a steel-steel contact. For the influence of the solid thermal conductivity, the simulation focuses on the through-hardened AISI 52100 bearing steel, whose thermal conductivity was recently measured as 21 W/mK in contrast to the value of 46 W/mK widely used in TEHL simulation for a traction rig. For the influence of the lubricant thermal conductivity, its dependence on pressure and temperature was considered for traction prediction. Squalane was adopted as the lubricant because its thermal-physical properties have been measured with great efforts and fitted to physically sound rheological models, *e.g.* Carreau shear thinning model and free-

volume based viscosity models. The simulated traction curves are compared with the measurements from two traction rigs with squalane. The largest deviation is about 18.8%. The main conclusions are:

1. For through-hardened AISI 52100 steel, with the improper thermal conductivity of 46 W/mK rather than the new measured value of 21 W/mK, the temperature rise in the EHL film is underestimated, while the friction coefficient is overestimated.
2. The effect of solid thermal conductivity on traction depends on the entrainment speed and the resulting film thickness. At high speeds, the influence of solid thermal conductivity on traction is decreasing in the thermo-viscous regime, while its effect on the maximum friction coefficient is still noticeable in the traction curve.
3. The pressure dependence of lubricant thermal conductivity needs to be considered at high velocities and at high SRR conditions for traction prediction. Otherwise, the traction can be underestimated and the maximum temperature can be overestimated.
4. For the steel-steel contact, the thermal conductivities, either k_s or $k_{\mathrm{oil}}(p,T)$, are not important for inlet heating, the thermal reduction factor, and the EHL central film thickness.

Acknowledgements

The authors would like to thank Dr. Björling for providing the measured WAM traction curves with squalane. This work is partly supported by FVV-Research Association for Combustion Engines e.V., Germany, through Grant No. 6012773. The first two authors, Liu and Zhang, would like to acknowledge the China Scholarship Council (CSC) for providing the scholarship.

Nomenclature

a	Hertzian contact radius, m
c, c_1, c_2	Heat capacity of the lubricant, solid-1, and solid-2, respectively, J/(kgK)
d, D	Computation domain of the solids in depth, m, and dimensionless $D = d/a$
E'	Reduced Young's modulus of elasticity, $E' = 2/[(1-v_1^2)/E_1 + (1-v_2^2)/E_2]$, Pa
f	Friction coefficient, (-)
G	Dimensionless materials parameter, $G = \alpha E'$
G_{s}	Shear modulus of the material, Pa
h, H	Film thickness, m, and dimensionless $H = hR_{\mathrm{x}}/a^2$
h_{cen}	Central film thickness, m
h_{00}, H_{00}	Rigid central film thickness, m, and dimensionless $H_{00} = h_{00}R_{\mathrm{x}}/a^2$
$k_{\mathrm{oil}}, k_{\mathrm{s}}$	Thermal conductivity of the lubricant and the solid, respectively, W/(mK)
n	Power-law exponent of the lubricant in the shear thinning equation, (-)
p_{H}	Maximum Hertzian pressure, Pa
p, P	Pressure, Pa, and dimensionless $P = p/p_{\mathrm{H}}$
$R, R_{\mathrm{x}}, R_{\mathrm{y}}$	Spheres radius, and $R = R_{\mathrm{x}} = R_{\mathrm{y}}$, m
T_0	Temperature of the supplied oil and the solid body temperature, K
$T, \bar{T}$	Absolute temperature, K, and dimensionless $\bar{T} = T/T_0$
u_1, u_2	Velocities of surface 1 and 2, m/s, and dimensionless $U_{1,2} = u_{1,2}/u_{\mathrm{e}}$
u_{e}	Entraining surface velocity, m/s, i.e. $u_{\mathrm{e}} = (u_1 + u_2)/2$

U_{e}	Dimensionless speed parameter, $U_{\mathrm{e}} = \eta_0 u_{\mathrm{e}}/(E' R_x)$
w	Contact load, N
W	Dimensionless load, $W = w/(E' R_{\mathrm{x}}^2)$
x, y, z	Space coordinates, m
$x_{\mathrm{in}}, x_{\mathrm{out}}, X_{\mathrm{in}}, X_{\mathrm{out}}$	Domain boundary in *x*-direction, m, and dimensionless $X_{\mathrm{in,out}} = x_{\mathrm{in,out}}/a$
$y_{\mathrm{out}}, Y_{\mathrm{out}}$	Domain boundary in *y*-direction, m, and dimensionless $Y_{\mathrm{out}} = y_{\mathrm{out}}/a$
z_1, z_2	Coordinates in solid-1 and solid-2, m, and dimensionless $Z_{1,2} = z_{1,2}/a$ (solids)
X, Y, Z	Dimensionless coordinates $X = x/a$, $Y = y/a$, $Z = z/h$ (lubricant)
α	Pressure-viscosity coefficient, m^2/N
λ_{R}	Characteristic or relaxation time at a reference state, s
$\rho, \bar{\rho}$	Density, $\mathrm{kg/m}^3$, and dimensionless $\bar{\rho} = \rho/\rho_0$
ρ_0	Density at ambient pressure, $\mathrm{kg/m}^3$
μ	Low-shear viscosity of the lubricant, Pas, and dimensionless $\bar{\mu} = \mu/\eta_0$
η^*	Generalized Newtonian viscosity, Pas, and dimensionless $\bar{\eta}^* = \eta^*/\eta_0$
η_0	Lubricant viscosity at T_0 and at ambient pressure, Pas
$\tau, \bar{\tau}$	Shear stress, Pa, and dimensionless $\bar{\tau} = \tau/p_H$
τ_{L}	Lubricant limiting shear stress, Pa
$\tau_{\mathrm{x}}, \tau_{\mathrm{y}}, \tau_{\mathrm{e}}$	Shear rate in two directions, Pa, and composite, $\tau_{\mathrm{e}} = \sqrt{\tau_{\mathrm{x}}^2 + \tau_{\mathrm{x}}^2}$
$\dot{\gamma}_{\mathrm{x}}, \dot{\gamma}_{\mathrm{y}}, \dot{\gamma}_{\mathrm{e}}$	Shear rate in two directions, and composite, $\dot{\gamma}_{\mathrm{e}} = \sqrt{\dot{\gamma}_{\mathrm{x}}^2 + \dot{\gamma}_{\mathrm{y}}^2}$, s^{-1}, and the dimensionless form of $\dot{\gamma}_{\mathrm{e}}$ is $\dot{\Gamma}$
ξ	Slide-to-roll ratio, SRR, $\xi = (u_1 - u_2)/u_{\mathrm{e}}$, (-)
Λ	Limiting stress-pressure coefficient, (-)

References

1. Venner CH, Lubrecht AA. *Multi-level methods in lubrication*. Amsterdam: Elsevier; 2000.
2. Hamrock BJ, Dowson D. Isothermal elastohydrodynamic lubrication of point contacts: part III—fully flooded results. *J Lub Tech* 1977;*99*(2):264-75.
3. Katyal P, Kumar P. Central film thickness formula for shear thinning lubricants in EHL point contacts under pure rolling. *Tribol Int* 2012;*48*:113-21.
4. Björling M, Habchi W, Bair S, Larsson R, Marklund P. Towards the true prediction of EHL friction. *Tribol Int* 2013;*66*:19-26.
5. Gohar R. *Elastohydrodynamics*. World Scientific Publishing Company;2001.
6. Bair S. *High pressure rheology for quantitative elastohydrodynamics*. Amsterdam, The Netherlands:Elsevier;2019.
7. Bair S, Winer WO. A rheological model for elastohydrodynamic contacts based on primary laboratory data. *J Lub Tech* 1979;*101*(3):258-64.
8. Johnson KL, Tevaarwerk JL. Shear behaviour of elastohydrodynamic oil films. *Proceedings of the Royal Society of London. A. Mathematical and Physical Sciences* 1977;*356*(1685):215-36.
9. Bader N, Wang D, Poll G. Traction and local temperatures measured in an elastohydrodynamic lubrication contact. *IMechE J Eng Trib* 2017;*231*(9):1128-39.
10. Liu HC, Zhang BB, Bader N, Guo F, Poll G, Yang P. Crucial role of solid body temperature on elastohydrodynamic film thickness and traction. *Tribol Int* 2019;*131*:386-97.

11. Reddyhoff T, Schmidt A, Spikes H. Thermal Conductivity and Flash Temperature. *Tribol Lett* 2019;*67*(1):22.
12. Habchi W, Vergne P, Bair S, Andersson O, Eyheramendy D, Morales-Espejel GE. Influence of pressure and temperature dependence of thermal properties of a lubricant on the behaviour of circular TEHD contacts. *Tribol Int* 2010;*43*(10):1842-50.
13. Shirzadegan M, Björling M, Almqvist A, Larsson R. Low degree of freedom approach for predicting friction in elastohydrodynamically lubricated contacts. *Tribol Int* 2016;*94*:560-70.
14. Larsson R, Andersson O. Lubricant thermal conductivity and heat capacity under high pressure. *IMechE J Eng Trib* 2000;*214*(4):337-42.
15. Bair S, Andersson O, Qureshi FS, Schirru MM. New EHL modeling data for the reference liquids squalane and squalane plus polyisoprene. *Tribol Trans* 2018;*61*(2):247-55.
16. Björling M, Habchi W, Bair S, Larsson R, Marklund P. Friction reduction in elastohydrodynamic contacts by thin-layer thermal insulation. *Tribol Lett* 2014;*53*(2):477-486.
17. Zhu D. Thermal Reduction of EHL Film Thickness. *In: Wang QJ, Chung YW. (eds) Encyclopedia of Tribology*. Boston:Springer;2013.
18. Bair S. The rheological assumptions of classical EHL: What went wrong?. *Tribol Int* 2019;*131*:45-50.
19. Bair S, McCabe C, Cummings PT. Comparison of nonequilibrium molecular dynamics with experimental measurements in the nonlinear shear-thinning regime. *Phy Rev Lett* 2002; *88*(5):058302.
20. Yang P, Wen SZ. A generalized Reynolds equation for non-Newtonian thermal elastohydrodynamic lubrication. *ASME J Tribol* 1990;*112*(4):631-6.
21. Liu Y, Wang QJ, Bair S, Vergne P. A quantitative solution for the full shear-thinning EHL point contact problem including traction. *Tribol Lett* 2007;*28*(2):171-81.
22. Bair S. Reference liquids for quantitative elastohydrodynamics: selection and rheological characterization. *Tribol Lett* 2006;*22*(2):197-206.
23. Murnaghan FD. The compressibility of media under extreme pressures. *Proceedings of the national academy of sciences of the United States of America* 1944;*30*(9):244.
24. Bair S, Mary C, Bouscharain N, Vergne P. An improved Yasutomi correlation for viscosity at high pressure. *IMechE J Eng Trib* 2013;*227*(9):1056-60.
25. Yang P. Thermal EHL Theory. *In: Wang QJ, Chung YW. (eds) Encyclopedia of Tribology*. Boston:Springer;2013.
26. Guo F, Yang P, Qu S. On the theory of thermal elastohydrodynamic lubrication at high slide-roll ratios—circular glass-steel contact solution at opposite sliding. *ASME J Tribol* 2001;*123*(4):816-21.
27. Habchi W. *A Full-system finite element approach to elastohydrodynamic lubrication problems* [Ph.D thesis]. INSA. Lyon, France;2008.
28. Bair S, Vergne P, Querry M. A unified shear-thinning treatment of both film thickness and traction in EHD. *Tribol Lett* 2005;*18*(2):145-52.
29. Björling M, Habchi W, Bair S, Larsson R, Marklund P. Corrigendum to "Towards the true prediction of EHL friction" [Tribol. Int. 66 (2013) 19–26]. *Tribol Int* 2019;*133*: 297.
30. Poll G, Wang D. Fluid rheology, traction/creep relationships and friction in machine elements with rolling contacts. *IMechE J Eng Trib* 2012;*226*(6):481-500.
31. Bair S, Kotzalas M. The contribution of roller compliance to elastohydrodynamic traction. *Tribol Trans* 2006;49(2):218-24.
32. Kaneta M, Yang P, Krupka I, Hartl M. Fundamentals of thermal elastohydrodynamic lubrication in Si3N4 and steel circular contacts. *IMechE J Eng Trib* 2015;*229*(8):929-39.

33. Wilzer J, Lüdtke F, Weber S, Theisen W. The influence of heat treatment and resulting microstructures on the thermophysical properties of martensitic steels. *J Mater Sci* 2013;*48*(24):8483-92.
34. Mustak O, Evcil E, Simsir C. Simulation of through-hardening of SAE 52100 steel bearings–Part I: Determination of material properties. *Materialwissenschaft und Werkstofftechnik* 2016;*47*(8):735-45.
35. Habchi W, Bair S. The role of the thermal conductivity of steel in quantitative elastohydrodynamic friction. *Tribol Int* 2020;*142*:105970.
36. Kaneta M, Yang P. Effects of thermal conductivity of contacting surfaces on point EHL contacts. *ASME J Tribol* 2003;*125*(4):731-8.
37. Kaneta M, Yang P. Effects of the thermal conductivity of contact materials on elastohydrodynamic lubrication characteristics. *IMechE J Eng Trib* 2010;*224*(12):2577-87.

Appendix 1. Governing equations for thermal EHL of steady-state

1 EHL part for a point contact

1.1 Generalized Reynolds equation

For the modelling of thermal and/or non-Newtonian aspects of EHL, density and viscosity should be allowed to vary across the thin film (in z-direction). Generalized Reynolds equation proposed by Yang and Wen [20] was used here for this purpose.

$$\frac{\partial}{\partial x}\left[\left(\frac{\rho}{\eta}\right)_{\mathrm{e}} h^3 \frac{\partial p}{\partial x}\right] + \frac{\partial}{\partial y}\left[\left(\frac{\rho}{\eta}\right)_{\mathrm{e}} h^3 \frac{\partial p}{\partial y}\right] = 12u_{\mathrm{e}} \frac{\partial(\rho^* h)}{\partial x} \tag{A1}$$

with boundary conditions

$$\begin{cases} p(x_{\mathrm{in}}, y) = p(x_{\mathrm{out}}, y) = p(x, \pm y_{\mathrm{out}}) = 0 \\ p(x, y) \geq 0 (x_{\mathrm{in}} < x < x_{\mathrm{out}}, -y_{\mathrm{out}} < y < y_{\mathrm{out}}) \end{cases} \tag{A2}$$

1.2 Film thickness equation

$$h(x, y) = h_{00} + \frac{x^2}{2R_{\mathrm{x}}} + \frac{y^2}{2R_{\mathrm{y}}} + \frac{2}{\pi E'} \iint \frac{p(x', y')}{\sqrt{(x - x')^2 + (y - y')^2}} \mathrm{d}x' \mathrm{d}y' \tag{A3}$$

1.3 Load balance equation

$$\iint p(x, y) \mathrm{d}x \mathrm{d}y = w \tag{A4}$$

1.4 Friction coefficient

The friction coefficient at rolling/sliding conditions is defined as the average value of traction coefficients of the upper and the lower surfaces [21]

$$f = -\frac{1}{2w} \iint \left(\eta^* \left(\frac{\partial u}{\partial z}\right)\Big|_{z=0} + \eta^* \left(\frac{\partial u}{\partial z}\right)\Big|_{z=h} \right) \mathrm{d}x \mathrm{d}y \tag{A5}$$

2 Thermal part

2.1 Oil energy equation [25]

$$c\left[\rho u\frac{\partial T}{\partial x}+\rho v\frac{\partial T}{\partial y}-\left(\frac{\partial}{\partial x}\int_0^z \rho u\mathrm{d}z'+\frac{\partial}{\partial y}\int_0^z \rho v\mathrm{d}z'\right)\frac{\partial T}{\partial z}\right]-k_{\mathrm{oil}}\frac{\partial^2 T}{\partial z^2}$$
$$=-\frac{T}{\rho}\frac{\partial \rho}{\partial T}\left(u\frac{\partial p}{\partial x}+v\frac{\partial p}{\partial y}\right)+\eta^*\left[\left(\frac{\partial u}{\partial z}\right)^2+\left(\frac{\partial v}{\partial z}\right)^2\right] \tag{A6}$$

k_{oil} is the thermal conductivity of the lubricant, which usually doubles its value at a pressure of 1 GPa. The temperature of the inlet boundary is set to the supplied oil temperature,

$$T(x_{\mathrm{in}},y,z)=T_0 \ \ (\mathrm{if}\, u(x_{\mathrm{in}},y,z)\geq 0) \tag{A7}$$

2.2 Solid energy equation

$$\begin{cases} c_1\rho_1 u_1\dfrac{\partial T}{\partial x}=k_{\mathrm{s1}}\dfrac{\partial^2 T}{\partial z_1^2} \\ c_2\rho_2 u_2\dfrac{\partial T}{\partial x}=k_{\mathrm{s2}}\dfrac{\partial^2 T}{\partial z_2^2} \end{cases} \tag{A8}$$

k_{s1} and k_{s2} are the thermal conductivities of the two solid surfaces. In this study, they are bearing steel. In TEHL literature, a value of 46 W/mK was widely used, while the new measured value is 21 W/mK for hardened bearing steel [11]. The resulting influences on EHL friction are simulated in this work. For pure sliding, the heat conduction in *x* and *y* directions should also be considered [25], which is not the case of the current study. The solid body temperature is assumed to be the same as the supplied oil temperature and the boundary conditions are

$$\begin{cases} T(x_{\mathrm{in}},y,z_1)=T_0, & T(x,y,h+d)=T_0 \\ T(x_{\mathrm{in}},y,z_2)=T_0, & T(x,y,-d)=T_0 \end{cases} \tag{A9}$$

Note that the boundary conditions in Eqs.(A8) and (A9) are seldom true for the modelling of the rolling/sliding contact in a traction machine, as during measurements the mass temperature of the disc is usually different from the supplied oil temperature T_0. This kind of solid body temperature effect is not important for this study. However, for quantitative traction prediction, it should be considered and this can be achieved by using the mass temperature of the solid instead of the supplied oil temperature T_0 in Eqs. (A8) and (A9), see Ref.[10].

2.3 Heat flux continuity on the oil/solid interface

$$k_{\mathrm{s1}}\frac{\partial T}{\partial z_1}\Big|_{z_1=0}=k_{\mathrm{oil}}\frac{\partial T}{\partial z}\Big|_{z=0}, k_{\mathrm{s2}}\frac{\partial T}{\partial z_2}\Big|_{z_2=0}=k_{\mathrm{oil}}\frac{\partial T}{\partial z}\Big|_{z=h} \tag{A10}$$

Research highlights

1) The widely cited thermal conductivity value of hardened AISI-52100 steel may be wrong.
2) The specimens of traction machine are usually made of through-hardened 52100 steel.
3) A thermal EHL model was built for reference liquids with physically-sound fluid models.
4) k_{solid} and k_{oil} affect temperature rise and traction prediction, but in two different ways.
5) The effect of solid thermal conductivity on traction depends on speed and film thickness.

Declaration of interests

☒ The authors declare that they have no known competing financial interests or personal relationships that could have appeared to influence the work reported in this paper.

☐The authors declare the following financial interests/personal relationships which may be considered as potential competing interests: